THE VOLTAGE-GATED SODIUM CHANNEL BETA4 SUBUNIT MAINTAINS EPITHELIAL PHENOTYPE IN MAMMARY CELLS

Adélaïde Doray, Roxane Lemoine, Marc Severin, Stéphanie Chadet, Osbaldo Lopez-Charcas, Audrey Héraud, Christophe Baron, Pierre Besson, Arnaud Monteil, Stine Falsig Pedersen, et al.

Cell Reports

THE VOLTAGE-GATED SODIUM CHANNEL BETA4 SUBUNIT MAINTAINS EPITHELIAL PHENOTYPE IN MAMMARY CELLS

--Manuscript Draft--

Manuscript Number:	
Full Title:	THE VOLTAGE-GATED SODIUM CHANNEL BETA4 SUBUNIT MAINTAINS EPITHELIAL PHENOTYPE IN MAMMARY CELLS
Article Type:	Report
Keywords:	NaVβ4; epithelial phenotype; β-catenin; Epithelial-to-Mesenchymal Transition; mammary cells
Corresponding Author:	Sébastien Roger, PhD University of Tours: Universite de Tours Tours, Centre FRANCE
First Author:	Adélaïde DORAY
Order of Authors:	Adélaïde DORAY
	Roxane LEMOINE
	Marc SEVERIN
	Stéphanie CHADET
	Osbaldo LOPEZ-CHARCAS
	Audrey HÉRAUD
	Christophe BARON
	Pierre BESSON
	Arnaud MONTEIL
	Stine Falsig PEDERSEN
	Sébastien Roger, PhD
Abstract:	Summary The SCN4B gene, encoding for the NaVβ4 subunit of voltage-gated sodium channels, was recently found to be expressed in normal epithelial cells and down-regulated in several cancers. However, its function in normal epithelial cells is not characterized. In this study, we demonstrate that reducing NaVβ4 expression in MCF10A non-cancer mammary epithelial cells generates important morphological changes observed both in two-dimensional cultures and in three-dimensional cysts. Most notably the loss of NaVβ4 induces a complete loss of epithelial organisation in cysts and increases proteolytic activity towards the extracellular matrix. Loss of epithelial morphology was associated with an increased degradation of β-catenin, reduced E-cadherin expression and induction of mesenchymal markers N-cadherin, vimentin, α-SMA expression. Overall, our results suggest that Navβ4 may participate in the maintenance of the epithelial phenotype in mammary cells and that its down regulation might be a determining step in early carcinogenesis.
Suggested Reviewers:	Raphael Rappetti-Mauss, PhD University of Nice Sophia Antipolis: Universite Cote d'Azur Raphael.RAPETTI-MAUSS@univ-cotedazur.fr Specialist of ion channels and cancer
	Philippe Chavrier, PhD Institut Curie philippe.chavrier@curie.fr Specialist of carcinogenesis and cancer progression
	Aubin Penna, PhD

	University of Poitiers: Universite de Poitiers aubin.penna@univ-poitiers.fr Specialist of ion channels and cancer
Opposed Reviewers:	

Cover Letter

Dr Sébastien Roger
Membre de l'Institut Universitaire de France
Director, EA4245 Transplantation, Immunologie, Inflammation
University of Tours
Faculty of Medicine, 10 boulevard Tonnellé
37032 Tours, France
E-mail : sebastien.roger@univ-tours.fr
Tel: 0033 2 47 36 61 30

Tours, 7th May 2021

Dear Editors of the journal *Cell Reports*,

Please find enclosed our manuscript entitled "**THE VOLTAGE-GATED SODIUM CHANNEL BETA4 SUBUNIT MAINTAINS EPITHELIAL PHENOTYPE IN MAMMARY CELLS**" that we would like to submit as a report article to the journal *Cell Reports*.

$Na_V\beta$ proteins are classically known to regulate the activity, the membrane trafficking and pharmacological properties of pore-forming subunits of voltage-gated sodium channels ($Na_V\alpha$) (Calhoun and Isom, 2014, Lenkowski et al., 2003, Zhang et al., 2013, Wilson et al., 2011). However, it recently appeared that $Na_V\beta$ proteins also have specific cellular functions in excitable cells expressing $Na_V\alpha$ isoforms, such as an important role as cell adhesion molecules (Isom, 2001, Isom, 2002). The most recently identified $Na_V\beta4$ subunit, encoded by the *SCN4B* gene, is the least characterized member of the family. It was initially demonstrated to be expressed in the nervous system (dorsal root ganglia, spinal cord and restricted areas or nuclei in the brain), in skeletal and cardiac muscle cells (Yu et al., 2003), in which it modulates $Na_V\alpha$ activity (Grieco et al., 2005, Miyazaki et al., 2014, White et al., 2019, Aman et al., 2009, Bant and Raman, 2010). Recently, we identified a critical role for $Na_V\beta4$ in cancer progression (Bon et al., 2016). Specifically, we have shown that $Na_V\beta4$ was strongly expressed in normal epithelial cells and tissues from breast, colon, rectum, lung and prostate but consistently downregulated in cancer samples, to be almost absent in high-grade primary and metastatic tumours (Bon et al., 2016). In mammary cancer cells, reducing $Na_V\beta4$ expression potentiated cell migration and invasiveness which resulted in an increase in mammary tumour growth and a higher metastatic colonisation. This effect was independent of $Na_V\alpha$ channel activity (Bon et al., 2016). It was suggested that the *SCN4B* gene might be considered as a metastasis-suppressor gene (Bon et al., 2016). Nevertheless, the function of $Na_V\beta4$ in normal epithelial cells is not known.

In this study, we demonstrate that reducing $Na_V\beta4$ expression in non-cancer mammary epithelial cells generates important morphological changes observed both in two-dimensional cultures and in three-dimensional cysts. Most notably the loss of $Na_V\beta4$ induces a complete loss of epithelial organisation in cysts and increases proteolytic activity towards the extracellular matrix. Loss of epithelial morphology was associated with an increased degradation of β-catenin, reduced E-cadherin expression and induction of mesenchymal markers N-cadherin, vimentin, α-SMA expression. In conclusions, our results highlight an important role for $Na_V\beta4$ in maintaining the epithelial phenotype in mammary cells. $Na_V\beta4$ down regulation might be a determining step in early carcinogenesis.
We do believe that these results are of high importance for the basic and translational research readership of the journal *Cell Reports*.

All authors have read and approved submission of the manuscript, and declare no conflict of interest.
The material presented in the manuscript has not been published and is not being considered for publication in whole or in part in any language. Thank you for considering our manuscript for publication.

Sincerely yours,

On behalf of all the authors,

Dr. Sébastien Roger

References presented in this cover letter:

AMAN, T. K., GRIECO-CALUB, T. M., CHEN, C., RUSCONI, R., SLAT, E. A., ISOM, L. L. & RAMAN, I. M. 2009. Regulation of persistent Na current by interactions between beta subunits of voltage-gated Na channels. *J Neurosci,* 29**,** 2027-42.

BANT, J. S. & RAMAN, I. M. 2010. Control of transient, resurgent, and persistent current by open-channel block by Na channel beta4 in cultured cerebellar granule neurons. *Proc Natl Acad Sci U S A,* 107**,** 12357-62.

BON, E., DRIFFORT, V., GRADEK, F., MARTINEZ-CACERES, C., ANCHELIN, M., PELEGRIN, P., CAYUELA, M. L., MARIONNEAU-LAMBOT, S., OULLIER, T., GUIBON, R., FROMONT, G., GUTIERREZ-PAJARES, J. L., DOMINGO, I., PIVER, E., MOREAU, A., BURLAUD-GAILLARD, J., FRANK, P. G., CHEVALIER, S., BESSON, P. & ROGER, S. 2016. SCN4B acts as a metastasis-suppressor gene preventing hyperactivation of cell migration in breast cancer. *Nat Commun,* 7**,** 13648.

CALHOUN, J. D. & ISOM, L. L. 2014. The role of non-pore-forming beta subunits in physiology and pathophysiology of voltage-gated sodium channels. *Handb Exp Pharmacol,* 221**,** 51-89.

GRIECO, T. M., MALHOTRA, J. D., CHEN, C., ISOM, L. L. & RAMAN, I. M. 2005. Open-channel block by the cytoplasmic tail of sodium channel beta4 as a mechanism for resurgent sodium current. *Neuron,* 45**,** 233-44.

ISOM, L. L. 2001. Sodium channel beta subunits: anything but auxiliary. *Neuroscientist,* 7**,** 42-54.

ISOM, L. L. 2002. The role of sodium channels in cell adhesion. *Front Biosci,* 7**,** 12-23.

LENKOWSKI, P. W., SHAH, B. S., DINN, A. E., LEE, K. & PATEL, M. K. 2003. Lidocaine block of neonatal Nav1.3 is differentially modulated by co-expression of beta1 and beta3 subunits. *Eur J Pharmacol,* 467**,** 23-30.

MIYAZAKI, H., OYAMA, F., INOUE, R., AOSAKI, T., ABE, T., KIYONARI, H., KINO, Y., KUROSAWA, M., SHIMIZU, J., OGIWARA, I., YAMAKAWA, K., KOSHIMIZU, Y., FUJIYAMA, F., KANEKO, T., SHIMIZU, H., NAGATOMO, K., YAMADA, K., SHIMOGORI, T., HATTORI, N., MIURA, M. & NUKINA, N. 2014. Singular localization of sodium channel beta4 subunit in unmyelinated fibres and its role in the striatum. *Nat Commun,* 5**,** 5525.

WHITE, H. V., BROWN, S. T., BOZZA, T. C. & RAMAN, I. M. 2019. Effects of FGF14 and NaVbeta4 deletion on transient and resurgent Na current in cerebellar Purkinje neurons. *J Gen Physiol,* 151**,** 1300-1318.

WILSON, M. J., ZHANG, M. M., AZAM, L., OLIVERA, B. M., BULAJ, G. & YOSHIKAMI, D. 2011. Navbeta subunits modulate the inhibition of Nav1.8 by the analgesic gating modifier muO-conotoxin MrVIB. *J Pharmacol Exp Ther,* 338**,** 687-93.

YU, F. H., WESTENBROEK, R. E., SILOS-SANTIAGO, I., MCCORMICK, K. A., LAWSON, D., GE, P., FERRIERA, H., LILLY, J., DISTEFANO, P. S., CATTERALL, W. A., SCHEUER, T. & CURTIS, R. 2003. Sodium channel beta4, a new disulfide-linked auxiliary subunit with similarity to beta2. *J Neurosci,* 23**,** 7577-85.

ZHANG, M. M., WILSON, M. J., AZAM, L., GAJEWIAK, J., RIVIER, J. E., BULAJ, G., OLIVERA, B. M. & YOSHIKAMI, D. 2013. Co-expression of Na(V)beta subunits alters the kinetics of inhibition of voltage-gated sodium channels by pore-blocking mu-conotoxins. *Br J Pharmacol,* 168**,** 1597-610.

Title page

THE VOLTAGE-GATED SODIUM CHANNEL BETA4 SUBUNIT MAINTAINS EPITHELIAL PHENOTYPE IN MAMMARY CELLS

Adélaïde DORAY[1], Roxane LEMOINE[1], Marc SEVERIN[2], Stéphanie CHADET[1], Osbaldo LOPEZ-CHARCAS[1], Audrey HÉRAUD[1], Christophe BARON[1], Pierre BESSON[1], Arnaud MONTEIL[3], Stine Falsig PEDERSEN[2] & Sébastien ROGER[1,4§]

[1] University of Tours, EA4245 Transplantation, Immunology, Inflammation, Tours, France

[2] Section for Cell Biology and Physiology, Department of Biology, Faculty of Science, University of Copenhagen, Copenhagen, Denmark

[3] IGF, University of Montpellier, CNRS, INSERM, Montpellier, France

[4] Institut Universitaire de France, Paris, France

[§]Correspondence: Dr. Sébastien Roger,
EA4245 Transplantation, Immunology, Inflammation, 10 Bd Tonnellé, 37032 Tours, France
Tel: (+33) 2 47 36 61 30, Email: sebastien.roger@univ-tours.fr

Running head: Naᵥβ4 as a gatekeeper of epithelial phenotype

Summary

The *SCN4B* gene, encoding for the Naνβ4 subunit of voltage-gated sodium channels, was recently found to be expressed in normal epithelial cells and down-regulated in several cancers. However, its function in normal epithelial cells is not characterized. In this study, we demonstrate that reducing Naνβ4 expression in MCF10A non-cancer mammary epithelial cells generates important morphological changes observed both in two-dimensional cultures and in three-dimensional cysts. Most notably the loss of Naνβ4 induces a complete loss of epithelial organisation in cysts and increases proteolytic activity towards the extracellular matrix. Loss of epithelial morphology was associated with an increased degradation of β-catenin, reduced E-cadherin expression and induction of mesenchymal markers N-cadherin, vimentin, α-SMA expression. Overall, our results suggest that Navβ4 may participate in the maintenance of the epithelial phenotype in mammary cells and that its down regulation might be a determining step in early carcinogenesis.

Key words: Naνβ4, epithelial phenotype, β-catenin, Epithelial-to-Mesenchymal Transition, mammary cells

Introduction

Voltage-gated sodium channels β (Naᵥβ) proteins, encoded by *SCNxB* genes, define a family of four transmembrane proteins with a short C-terminal intracellular domain and a large N-terminal Immunoglobulin (Ig)-like extracellular domain (Brackenbury and Isom, 2011). These proteins have initially been characterized as auxiliary subunits of sodium channels (Messner and Catterall, 1985). Indeed, they were isolated along with pore-forming voltage-gated sodium channel (Naᵥα) isoforms, which they interact with through covalent or non-covalent associations (McCormick et al., 1998, Meadows et al., 2001, Chen et al., 2012, Gilchrist et al., 2013). Hence, Naᵥβ proteins regulate Naᵥα membrane trafficking as well as their biophysical (Calhoun and Isom, 2014) and pharmacological properties (Lenkowski et al., 2003, Zhang et al., 2013, Wilson et al., 2011). Along with these roles as sodium channel activity modulators, Naᵥβ proteins have also been proven to conduct other specific cellular functions in excitable cells (Isom, 2001), such as an important role as cell adhesion molecules (CAMs), allowing for both *trans*-homophilic and *trans*-heterophilic cell-cell and cell-matrix adhesions in cells expressing Naᵥα isoforms (Isom, 2002). Therefore, the expression and roles of Naᵥβ are best known in excitable cells such as in neurons in which they participate in the regulation of Na^+ influx but also control neurite outgrowth, axonal fasciculation and interaction with glial cells (O'Malley and Isom, 2015).

The most recently identified Naᵥβ4 subunit, encoded by the *SCN4B* gene, is the least characterized member of the family. It was initially demonstrated to be expressed in the nervous system (dorsal root ganglia, spinal cord and restricted areas or nuclei in the brain), in skeletal and cardiac muscle cells (Yu et al., 2003). It shares sequence similarity with the Naᵥβ2 subunit and engages in covalent interactions with Naᵥα in the extracellular Ig domain (Yu et al., 2003, Gilchrist et al., 2013). Naᵥβ4 was demonstrated to control Naᵥα activity and particularly the generation of resurgent (Grieco et al., 2005, Miyazaki et al., 2014, White et al., 2019) or persistent (Aman et al., 2009, Bant and Raman, 2010) sodium currents in neurons. Naᵥβ4 was also identified to participate in cell-cell adhesion (Shimizu et al., 2017) and neurite extension (Miyazaki et al., 2007). Evidence is shown that Naᵥβ4

dysregulation is involved in epilepsy (Sheilabi et al., 2020), in Rett Syndrome (Oginsky et al., 2017) and mutations in the *SCN4B* gene have been linked to cardiac arrythmia (Li et al., 2013, Yang et al., 2019, Xiong et al., 2019, Medeiros-Domingo et al., 2007) and sudden death syndromes (Tan et al., 2010).

Recently, we identified a critical role for Na$_V$β4 in cancer progression (Bon et al., 2016). Specifically, we have shown that Na$_V$β4 was strongly expressed in normal epithelial cells and tissues from breast, colon, rectum, lung and prostate but consistently downregulated in cancer samples, to be almost absent in high-grade primary and metastatic tumours (Bon et al., 2016). In mammary cancer cells, reducing Na$_V$β4 expression potentiated cell migration and invasiveness through the acquisition of a hybrid mesenchymal-amoeboid aggressive phenotype which resulted in an increase in mammary tumour growth and a higher metastatic colonisation. This effect was independent of Na$_V$α channel activity (Bon et al., 2016). Later on, similar results were obtained in cervical cancer cells (Sanchez-Sandoval and Gomora, 2019) and the preserved expression of *SCN4B* in papillary thyroid cancer was proposed to be a favourable indicator of recurrence-free survival (Gong et al., 2018). It was therefore suggested that the *SCN4B* gene might be considered as a metastasis-suppressor gene (Bon et al., 2016). Nevertheless, the function of Na$_V$β4 in normal epithelial cells is not known. We therefore hypothesized that Na$_V$β4 is important for epithelial phenotype. To test this, we explored the consequences of reducing Na$_V$β4 expression in non-cancer MCF10A mammary cells. We show that knocking-down Na$_V$β4 induced a loss of epithelial phenotype that is reminiscent to early stages of carcinogenesis.

Results

Bioinformatics gene expression analyses, using The Cancer Genome Atlas (TCGA) and the UCSC Xena browser (https://xenabrowser.net), confirmed initial studies (Bon et al., 2016) indicating that the *SCN4B* gene, encoding for Na$_V$β4, is significantly down-regulated in all breast cancer stages compared to adjacent non-tumoral breast tissues (Fig. 1a). A lower expression of *SCN4B* was even identified in stage IIA compared to stage I (Fig. 1a). In line with these initial results, Na$_V$β4 protein expression was almost 10 times lower in human mammary cancer MDA-MB-231 compared to non-cancer MCF10A cells (Fig. 1b). In order to assess the potential role of Na$_V$β4 in non-cancer mammary cells we developed, using the CRISPR/Cas9 technique, a cell line derived from the parental MCF10A with a permanent knockdown of Na$_V$β4, named MCF10A Crβ4, as well as a control cell line MCF10A CTL. The efficiency of Na$_V$β4 knock-down was verified by western blotting indicating a median reduction of protein expression of 85% (Fig. 1c). Reduction of Na$_V$β4 had important effects on MCF10A cell morphology, as observed in conventional 2-dimensional cultures (Fig. 1d). Particularly, MCF10A Crβ4 showed an elongated morphology characterised by an increased cell length as compared with MCF10A CTL (Fig. 1e, 89.9 ± 5.1 *vs*. 33.1 ± 1.7 µm, respectively). Furthermore, while MCF10A CTL cells showed a tendency for being closely associated in clusters, as epithelial cells do, MCF10A Crβ4 were more scattered and established less intercellular interactions (Fig. 1f). These morphological changes were also identified by epifluorescence imaging in fixed cells labelled to visualize cell nuclei and F-actin network (Fig. 1g). Image analysis demonstrated that MCF10A Crβ4 showed a greater cell surface than MCF10A CTL cells (Fig. 1h, 2,318 ± 123 *vs*. 1,062 ± 52 µm^2, respectively). Interestingly, MCF10A Crβ4 also appeared to have a stronger intensity of F-actin labelling (Fig. 1i), characterised by the presence of actin stress fibres (Fig. 1g).

These initial data suggested that the loss of Na$_V$β4 expression affected epithelial cell phenotype and intercellular organization. We next investigated how the loss of Na$_V$β4 affected cell polarisation in 3 dimensions, using a cyst forming assay in a 3D extracellular matrix (Jensen et al., 2018). We found

that, in 3D cultures, MCF10A CTL cells formed regular cysts with a general spheroid morphology (Fig. 2a), characterized by a circularity index (calculated from pictures) approaching 0.9, maintained during the 3 weeks of the experiment (Fig. 2b). MCF10A CTL cysts demonstrated a regular growth that was slightly slowed after 14 days culture (Fig. 2c). After this time, the number of remaining individualized cysts tended to decrease, mostly due to the dispersion of some cells into the extracellular matrix (Fig. 2d). MCF10A Crβ4 cysts also exhibited a generally spheroid shape, albeit demonstrating a lower circularity index (Fig. 2a, b), but their growth was slower compared to MCF10A CTL cysts (Fig. 2c). This could be partly due to a reduced cell proliferation rate. Indeed, loss of $Na_V\beta4$ expression slightly reduced MCF10A cell viability after 5 days of culture (Suppl. Fig. 1a) which appeared to be due to a slower DNA synthesis (Suppl. Fig. 1b, c). However, it also appeared that cells evaded from MCF10A Crβ4 cysts to invade the 3D extracellular matrix (Fig 2a, arrows), thus resulting in the complete disorganisation of cysts and in the reduction of the number of individualized cysts with time (Fig. 2a, d). We thus characterized cysts ultrastructure. Cysts were fixed and stained in order to visualise cell nuclei, vimentin expression and F-actin network by fluorescence imaging. MCF10A CTL cysts demonstrated a typical and regular epithelial organisation with compacted cell nuclei uniformly distributed within the structure, the expression of vimentin at the external periphery of the cyst (equivalent to the basal side of the epithelial layer), contiguous cells displaying a cortical submembrane F-actin network, and the appearance of a central lumen (Fig. 2e). By contrast, MCF10A Crβ4 cysts were completely disorganized, lacked a central lumen and did not show any apico-basal polarisation (Fig. 2e). Cell nuclei appeared to be less compacted, vimentin expression was more intense and diffuse, and cortical F-actin network was disrupted to be more diffuse inside the cytosol. Furthermore, multiple cells detached from the cyst to invade the extracellular matrix. Because this property might require proteolytic activities, we explored the capacity of MCF10A cysts to degrade the fluorogenic substrate DQ-Gelatin when incorporated into the extracellular matrix, after 7 days growing (Fig. 2f). MCF10A CTL cysts demonstrated almost undetectable proteolytic activity. By contrast MCF10A Crβ4 cysts showed a strong proteolytic

activity towards the extracellular matrix (green fluorescence) and a strong invasion by cells originating from the cyst (Fig 2f, g). Because cell-cell junctions appeared to be disrupted in MCF10A Crβ4 cysts, we then analysed the expression of adherens junction proteins β-catenin and E-cadherin. While MCF10A CTL cysts were characterized by a strong colocalization of β-catenin and E-cadherin at the plasma membrane of cells, MCF10A Crβ4 cysts demonstrated a weaker and diffuse expression of both proteins with no colocalization (Fig. 3a). These observations prompted us to investigate the expression of β-catenin depending on that of $Na_V\beta4$. Consistent with the more mesenchymal phenotype, the mRNA level of gene encoding for β-catenin, *CTNNB1*, was significantly higher in MCF10A Crβ4 compared to MCF10A CTL cells (40% median increase, Fig. 3b). In contrast, β-catenin protein level was down-regulated in MCF10A Crβ4 compared to MCF10A CTL cells (52% median decrease, Fig. 3c). A possible explanation for this apparent discrepancy could be an increased recycling of β-catenin in MCF10A Crβ4 cells. Therefore, we incubated MCF10A CTL and MCF10A Crβ4 cells with the proteasome inhibitor MG132 for different time durations and assessed levels of β-catenin (Fig. 3d). These led to an increased immunodetection of β-catenin in both cell lines. Nevertheless, the increase in β-catenin protein expression was significantly higher in MCF10A Crβ4 than in MCF10A CTL cells (Fig. 3e). Similarly, MCF10A cells transfected with specific silencing RNA targeting $Na_V\beta4$ (siβ4, Fig. 3f) also displayed a reduced expression of β-catenin compared to scramble siRNA (siCTL, Fig. 3g) and this expression was restored upon treatment with MG132 (Fig. 3h). These results suggested that the loss of the plasma membrane $Na_V\beta4$ leads to the disruption of intercellular junctions and to a reduced half-life of β-catenin. Together with the loss of the epithelial morphology in individual cells, the disorganisation and the increased extracellular invasiveness of cysts, the disruption of adherens junctions argued in favour of a transition towards a mesenchymal-like phenotype. Therefore, we next examined the expression of genes associated with either epithelial phenotype (*CDH1*, encoding for E-cadherin) or with mesenchymal phenotype (*CDH2*, encoding for N-cadherin; *SNAI1, SNAI2, TWIST, ZEB1* encoding for transcription factors promoting epithelial-to-mesenchymal transition, *VIM*, encoding for vimentin, and *ACTA2*, encoding for α-SMA). The loss of

$Na_V\beta4$ expression was associated with a significant reduction in the epithelial marker *CDH1* expression, and an increase in the expression of mesenchymal markers *CDH2*, *SNAI2*, *TWIST*, *ZEB1*, *VIM* and *ACTA2* (Fig. 4a). Only *SNAI1* expression was not modified. These changes observed at the transcriptional level were confirmed at the protein level for E-Cadherin, N-Cadherin, Vimentin and α-SMA (Fig. 4b). Finally, we explored the possibility to rescue the epithelial phenotype in MCF10A Crβ4 by overexpressing $Na_V\beta4$ (Fig. 4c). This partially restored *CDH2*, *VIM* and *ACTA2* expression (Fig. 4d).

Discussion

Pore-forming $Na_V\alpha$ and auxiliary $Na_V\beta$ proteins of voltage-gated sodium channels were initially characterized in excitable cells in which they are responsible for the triggering and the propagation of action potentials. However, over the past years it has been shown that both $Na_V\alpha$ and $Na_V\beta$ subunits are dysregulated in cancers, in which they have non-excitable roles. Most of the time, their overexpression in carcinoma cells has been associated with cancer progression, and their activity was shown to promote pro-cancerous properties (Lopez-Charcas et al., 2021). Pore-forming $Na_V1.5$, $Na_V1.6$ and $Na_V1.7$ appear to be specifically up-regulated in cancer cells and their activity, through an inward sodium current, has been shown to promote invasive properties (Roger et al., 2015). It has also been found that some $Na_V\beta$ subunits are up-regulated in cancer and that they bear important roles in cancer cell biology and in cancer progression (Lopez-Charcas et al., 2021). In contrast, the $Na_V\beta4$ subunit has recently been identified as being expressed at high levels in normal epithelial tissues, but consistently down-regulated in cancer samples. This was identified in breast, lung, prostate and colorectal cancer (Bon et al., 2016), in cervical cancer (Sanchez-Sandoval and Gomora, 2019) and in papillary thyroid cancer (Gong et al., 2018). In these studies, the preserved expression of the *SCN4B* gene was considered as a favourable biomarker of metastasis-free survival suggesting that it could be a metastasis-suppressor gene.

The expression of the *SCN4B* gene was shown to be lower in highly invasive cancer as compared to weakly invasive or to non-cancer cells (Bon et al., 2016, Sanchez-Sandoval and Gomora, 2019, Roger et al., 2007). Both *in vitro* and *in vivo* experiments, performed with different human cancer cell lines, demonstrated that reducing $Na_V\beta4$ expression potentiated cell migration, invasiveness and tumour progression, while overexpressing it had opposite effects (Bon et al., 2016, Sanchez-Sandoval and Gomora, 2019, Diss et al., 2008). In breast cancer cells, the loss of $Na_V\beta4$ promoted RhoA activity and the acquisition of a hybrid mesenchymal-amoeboid phenotype associated with highly invasive capacities (Bon et al., 2016). However, the role of $Na_V\beta4$ in normal epithelial cells is not known, and whether its loss might participate to events of early carcinogenesis has never been characterized.

In this study, we confirmed that *SCN4B* / Na$_V$β4 is down-regulated in cancer compared to non-cancer cells and tissues. Furthermore, we demonstrated that its repression in non-cancer mammary epithelial cells induced dramatic morphological and functional changes associated with a loss of epithelial polarisation, a disruption of epithelial junctions, the overexpression of genes associated with a mesenchymal phenotype and the acquisition of pro-invasive capacities. Consequently, loss of Na$_V$β4 completely abrogated the establishment of 3D epithelial structures (cysts). The loss of Na$_V$β4 favoured the degradation of β-catenin, thus reducing its half-life and leading to the disruption of adherens junctions. It can be speculated that the Na$_V$β4 subunit, expressed at the plasma membrane of epithelial cells, stabilizes β-catenin in proximity with E-cadherin. Loss of Na$_V$β4 might lead to cytosolic release of β-catenin which could, for one part translocate to the nucleus and induce the expression of EMT-related genes, and for a second part undergo proteasomal degradation. These cellular events might be critical during carcinogenesis.

However, what could trigger the repression of *SCN4B* during cancer transformation is still unknown. Interestingly, recent studies pointed out the involvement of several miRNAs that are dysregulated in some cancers, as important regulators of *SCN4B* expression. In colorectal cancer, the increased expression of miR-424-5p in tumour samples was associated with poor prognosis (Dai et al., 2020). In this study, the authors demonstrated that *SCN4B* was directly inhibited by miR-424-5p thus promoting colon cancer cell proliferation, migration and invasion (Dai et al., 2020). Another miRNA, miR-3175, has recently been shown to be overexpressed in prostate cancer and to participate in cancer cell growth and invasion. Knocking down miR-3175 in prostate cancer cells increased *SCN4B* and E-cadherin expression, inhibited N-cadherin expression, and importantly reduced cell proliferation, migration and invasion (Huang et al., 2021). Together, these recent studies brought new elements on the involvement of miRNA in the promotion of cancer progression through the regulation of *SCN4B* expression in tumours. As such, exploring the expression of these miRNAs during carcinogenesis might be of importance.

In conclusion, this study demonstrates the critical role played by $Na_V\beta4$ in the maintenance of an epithelial phenotype in normal cells, and how its repression might contribute to cellular dysplasia and early carcinogenesis. In this context, maintaining its expression level in epithelial cells would be determinant in order to prevent, or delay, tumour transformation.

Acknowledgements

This work was supported by the "Ministère de la Recherche et des Technologies", the "Ligue Nationale Contre le Cancer – Interrégion Grand-Ouest – comités 29, 36, 86, 37" to S.R., the Région Centre-Val de Loire (grant “NavMetarget”). S.R. was recipient of a prize “Prix Ruban Rose Avenir 2017” from the charity “le Cancer du sein: parlons-en!”. A.D. obtained a PhD fellowship from the University of Tours, and a mobility grant from the Doctoral School ED549. O.L.-C. was recipient of a post-doctoral funding from the “Fondation pour la Recherche Médicale (FRM)” (SPF201909009198). R.L. was funded by a grant from the Région Centre-Val de Loire (grant “CanalEx”) to S.R. We thank Mrs Carole Desplanches for secretary and administrative assistance. Our confocal microscopy data were obtained with the assistance of the IBiSA Electron Microscopy Facility of the University of Tours, and we are grateful to M. Julien Burlaud-Gaillard for his help.

Author contributions

All authors contributed extensively to the work presented in this study. A.D. performed cell culture, molecular and cellular biology experiments, immunofluorescence/confocal imaging. R.L. performed cell culture and flow cytometry experiments. M.S. performed cell culture, molecular and cellular biology experiments, and confocal imaging. S.C. and O.L-C. participated in cell culture, imaging, and bioinformatics analyses. A.H. participated to cell culture and EdU assays. C.B. and P.B. participated to scientific discussions and critical reading of the manuscript. A.M. designed overexpression plasmids. S.F.P. directed the work on cysts and associated imaging. S.R. obtained funding, directed the research, designed the study, analysed the data, and wrote the manuscript.

Declaration of Interest

The authors declare no competing interests.

Figure legends

Figure 1: Navβ4 downregulation induces morphological changes in non-cancer mammary cells

a, The expression level of the *SCN4B* gene, encoding for Navβ4, was analysed from datasets coming from the "The Cancer Genome Atlas" (http://cancergenome.nih.gov) from the US National Cancer Institute in non-tumoral adjacent tissue (n=178), and in the different stages of primary breast tumours : I (n=125), IIA (n=243), IIB (n=115), IIIA (n=85), IIIB (n=10), IIIC (n=31), IV (n=4). For each array, data were log2-transformed and centred to the median. *** statistically different at $p<0.001$ (Mann-Whitney rank sum test) when comparing to adjacent non-tumoral tissue, and * at $p<0.05$ when comparing Stage I to stage IIA. **b**, Navβ4 protein expression level was assessed by western blotting in non-cancer MCF10A human mammary epithelial cells and in human breast cancer MDA-MB-231 cells. The upper section shows a WB representative of 5 independent experiments. HSC70 immunodetection was used as a loading control. The lower section shows a quantification of Navβ4 protein expression in the two cell lines expressed relatively to that of MCF10A. * Statistically different at $p<0.05$ (Mann-Whitney rank sum test). **c**, Navβ4 protein expression level was assessed by western blotting in control MCF10A cells and in cells stably knocked-down for the expression of *SCN4B* gene (MCF10A Crβ4). The upper section shows a WB representative of 8 independent experiments. HSC70 immunodetection was used as a loading control. The lower section shows a quantification of Navβ4 protein expression in the two cell lines expressed relatively to that of MCF10A CTL (n=8). * Statistically different at $p<0.05$ (Mann-Whitney rank sum test). **d**, Representative images of MCF10A CTL and MCF10A Crβ4 cells in phase contrast microscopy. Scale bar, 50 µm. **e**) Maximal cell length (n=31 MCF10A CTL and n=20 MCF10A Crβ4) and, **f**, Number of intercellular contacts per cell (n=60 MCF10A CTL and n=57 MCF10A Crβ4), assessed from images taken as in (d). *** Statistically different at $p<0.001$ (Students t-test). **g**, MCF10A CTL and MCF10A Crβ4 cells were stained for the identification of nuclei (DAPI, blue staining) and F-actin (phalloidin-594, red staining). Scale bar, 50 µm. **h**, Mean cell area (n=40 MCF10A CTL and n=

40 MCF10A Crβ4), and **i**) F-actin fluorescence intensity per cell surface (n=100 MCF10A CTL and n= 100 MCF10A Crβ4) were calculated From images taken as in (g). *** Statistically different at $p<0.001$ (Students t-test).

Figure 2: Naνβ4 sustains epithelial polarity in 3-dimensional MCF10A cysts.

a, MCF10A CTL and MCF10A Crβ4 cells were grown as cysts for 21 days in a 3D matrix. Representative images at days 2, 7, 14 and 21 are shown. Black arrows show cells evading from cysts and invading the extracellular matrix. Scale bar, 150 μm. **b**, A cyst circularity index was calculated from same cysts that in (a). Statistically different from MCF10A CTL at *, $p<0.05$ (ANOVA test). **c**, The perimeter of individual cysts was measured as a function of time from same cysts than in (a). Statistically different from MCF10A CTL at *, $p<0.05$ and **, $p<0.01$ (ANOVA test). **d**, The number of individualized cysts was assessed as a function of time and expressed relatively to the initial number at day 1 (n= 50 and 83 MCF10A CTL and MCF10A Crβ4 cysts, respectively, from 6 independent experiments). Statistically different from MCF10A CTL at *, $p<0.05$ and **, $p<0.01$ (ANOVA test). **e**, MCF10A CTL and MCF10A Crβ4 cysts were then fixed and stained with Hoechst 33342 to visualize cell nuclei (blue staining), as well as with phalloidin-594 to visualize F-actin network (red staining). Cysts were also immunostained with a primary rabbit anti-vimentin antibody and a secondary AF488-coupled anti-rabbit antibody (green staining). The white asterisk indicates the presence of a lumen inside MCF10A CTL cysts. Representative images from 6 independent experiments. Scale bar, 25 μm. **f**, Proteolytic activity of cysts was assessed by including DQ-gelatin, which emits green fluorescence when degraded, in the 3D matrix. Representative images from 8 independent experiments. Scale bar, 150 μm. **g**, An index of DQ-gelatin degradation was calculated from images as in (f) from 16 individualized MCF10A CTL and 21 MCF10A Crβ4 cysts at day 7. Statistically different from MCF10A CTL cysts at **, $p<0.01$ (Student t-test).

Figure 3: Naνβ4 prevents β-catenin degradation

a, MCF10A CTL and MCF10A Crβ4 cysts were stained with Hoechst 33342 to visualize cell nuclei and immunostained to identify β-catenin and E-cadherin. Representative images from 6 independent experiments. Scale bar, 25 μm. **b**, Expression of the *CTNNB1* gene, encoding for β-catenin, was analysed in MCF10A CTL and MCF10A Crβ4 cells (n=8 independent experiments). Statistically different from MCF10A CTL cysts at ***, $p<0.001$ (Mann-Whitney rank sum test). **c**, Left, β-catenin protein expression level was assessed by western blotting in MCF10A CTL and MCF10A Crβ4 cells. Representative WB from 6 independent experiments. Right, quantification of β-catenin protein expression in MCF10A CTL and MCF10A Crβ4 cells (n=6). * Statistically different at $p<0.05$ (Mann-Whitney rank sum test). **d**, β-catenin protein expression was assessed in untreated (Unt) MCF10A CTL and MCF10A Crβ4 cells, or after the treatment with 10 μM MG132 for 3h, 6h, 12h or 24h, or the solvent DMSO. β-actin immunodetection was used as a loading control. **e**, Quantification of β-catenin protein expression in same conditions as in (d), from 5 independent experiments. Statistical difference at $p<0.001$ (Two-way ANOVA). **f**, Naνβ4 protein expression was assessed by western blotting in MCF10A transfected with control "irrelevant" siRNA (siCTL) or with *SCN4B*-specific siRNA (siβ4) at 5 and 30 nM. **g**, β-catenin protein expression was assessed in untreated MCF10A cells or in cells transfected with siCTL or siβ4 (30 nM). β-actin immunodetection was used as a loading control. Representative from 5 independent experiments. **h**, β-catenin protein expression was assessed in MCF10A cells transfected with siCTL or siβ4 (30 nM) after the treatment with 10 μM MG132 for 3h, 6h, 12h or 24h, or the solvent DMSO. β-actin immunodetection was used as a loading control.

Figure 4: Naνβ4 expression prevents mesenchymal transition in MCF10A epithelial mammary cells. a, Expression of genes associated with either epithelial (*CDH1*) or mesenchymal (*CDH2*, *SNAI1*, *SNAI2*, *TWIST*, *ZEB1*, *VIM*, *ACTA2*) phenotype by RT-qPCR in MCF10A CTL and MCF10A Crβ4 cells (n=5-9 independent experiments). Results are expressed relatively to that of MCF10A CTL cells. "ns" stands for no statistical difference. Statistically different at * $p<0.05$, ** $p<0.01$ (Mann-

Whitney rank sum test). **b**, Representative western blots showing the protein expression of E-cadherin, N-Cadherin, Vimentin, α-SMA in MCF10A CTL and MCF10A Crβ4 cells. Immunodetection of HSC70 was used as a loading control (n=4 independent experiments). **c**, Naᵥβ4 protein expression was assessed by western blotting in MCF10A Crβ4 cells transfected with empty pcDNA3.1 or *SCN4B* gene in pcDNA3.1 vector. Representative from 8 independent experiments. **d**, Expression of genes associated with either epithelial (*CTNNB1*, *CDH1*) or mesenchymal (*CDH2*, *SNAI1*, *SNAI2*, *TWIST*, *ZEB1*, *VIM*, *ACTA2*) phenotype by RT-qPCR in MCF10A Crβ4 cells transfected with empty pcDNA3.1 or *SCN4B* gene in pcDNA3.1 vector (n=8 independent experiments). Results are expressed relatively to that of cells transfected with the empty vector. Statistically different at * $p<0.05$ (Mann-Whitney rank sum test), otherwise no statistical difference.

STAR Methods

Bioinformatic analyses - Gene expression data were obtained from The Cancer Genome Atlas (TCGA) and Genotype-Tissue Expression (GTEx) databases using the UCSC Xena Browser (https://xenabrowser.net)[49]. The IlluminaHiSeq (log2-normalized_count+1) files were downloaded from the "TCGA Breast Cancer (TCGA-BRCA)" cohort, in order to compare expressions between adjacent non-tumoral tissues and primary tumour. From the "TCGA TARGET GTEx" cohort, the RSEM norm_count (log2-normalized_count+1) files were downloaded, in order to compare expressions between adjacent non-tumoral tissues, primary tumour and metastases.

Inhibitors and chemicals - The proteasome inhibitor MG132 as well as all chemicals were purchased from Sigma-Aldrich (France). Fluorescent probes DQ™-Gelatin and Hoechst 33342 were purchased from Invitrogen (France), and Phalloidin-AF594 from Cell Signaling Technology (France). ProLong® Gold Antifade Mountant containing DAPI was purchased from Invitrogen, (France).

Cells and cell culture – The human breast cancer cell line MDA-MB-231 and non-cancer mammary epithelial MCF10A cells were acquired from the American Type Culture Collection (ATCC), through LGC Standards (France), and were grown at 37°C in a humidified 5% CO_2 incubator. MDA-MB-231 cells were grown in Dulbecco's modified Eagle's medium (DMEM) supplemented with 5% foetal calf serum (FCS). The immortalized non-cancer mammary epithelial MCF10A cells were cultured in DMEM/Ham's F-12, 1:1 mix containing 5% horse serum (Dutscher, France), 10 µg/mL insulin, 20 ng/mL epidermal growth factor, 0.5 µg/mL hydrocortisone, and 100 ng/mL cholera toxin. A stable MCF10A cell line knocked-down for the expression of the *SCN4B* gene, encoding for Na$_V$β4, was generated using the CRISPR/Cas9 technique, as previously described (Brisson et al., 2020) by transfection with the *SCN4B* Double Nickase Plasmid (sc-411001, Santa Cruz, France). Transfection was performed using Lipofectamine 2000 (Invitrogen, France). Selection of a stable cell line called "MCF10A Crβ4" was performed using 10 µg/ml puromycin, and was compared to a control cell line, thereafter called "MCF10A CTL". Efficiency of the CRISPR-

mediated knock-down was assessed by western blotting and stability of cells was followed for a minimal duration of 6 weeks. Mycoplasma contamination tests were performed routinely (Lonza, MycoAlert™ Mycoplasma Detection Kit).

Small interfering RNA transfection – MCF10A mammary epithelial cells were transfected with siRNA directed against human *SCN4B* mRNA (siβ4) or scramble siRNA as a control (siCTL), both of which were purchased from ON-TARGETplus siRNA (Horizon Discovery, Cambridge, UK). Cells were transfected using Pepmute™ siRNA Transfection Reagent (SinaGen laboratories, USA). Experiments were performed 24h-48h after transfection and efficacy of silencing was assessed by western blotting.

Overexpression of SCN4B gene – MCF10A Crβ4 cells were transfected with 2 µg of a pcDNA3.1(+) plasmid containing the *SCN4B* gene (pc*SCN4B*, Synbio Technologies, USA) or with a pcDNA3.1(+) empty vector as a control. Transfection was realized using Lipofectamine 2000 (Invitrogen, France).

RNA extraction, reverse transcription (RT) and quantitative-polymerase chain reaction (qPCR) **–**Total RNA was extracted using TRIzol™ Reagent (Invitrogen, France), quantified by measuring absorbance at 260 nm using Nanodrop 2000™ (Thermofisher, France) and reverse-transcribed with the PrimeScript™ RT Reagent Kit (Takara Bio Group, France). Quantitative PCR were performed using SYBR qPCR Premix Ex Taq (Takara Bio Group, France) and LightCycler 384 wells (Roche, France). Control gene was *HPRT1*. All primers sequences and corresponding efficiencies are described in Supplementary Table I.

Cell viability **–** cell viability was evaluated by the tetrazolium salt assay (MTT) as already described (Jelassi et al., 2011). Briefly, cells were seeded in different densities indicated in the figure and grown for 4 days at 37°C and 5% CO_2 in their normal culture medium. Cell viability was measured after incubation with 0.5 mg/mL MTT for 60 minutes at 37°C by measuring the absorbance at 540 nm.

Cell proliferation – Cells were seeded at a density of $2x10^5$ in wells of a 6-well plate. 72h after seeding, medium was removed and cells were incubated in a fresh culture medium containing 10 µM 5-Ethynyl-2'deoxyuridine (EdU). Cells were then washed in phosphate-buffered saline (PBS), trypsinized and the incorporation of EdU was monitored by flow cytometry (BD FACS Canto, Becton Dickinson, France) using the Click-iT™ Plus EdU Alexa Fluor488 kit (Invitrogen, France).

Cysts production and analyses - A 40 µL layer of Geltrex® (Sigma-Aldrich, France) was added into the wells of Nunc™ Lab-Tek™ II Chamber Slide™ (Thermo Scientific) mimicking the extracellular matrix. The chamber slide was incubated at 37°C for 20 min. MCF10A CTL or MCF10A Crβ4 cell suspensions were prepared in medium containing 25 µL/mL Geltrex® and seeded at 10,000 cells per 400 µL in the chamber slide wells. The culture medium of cells was replaced every 2 days by 400 µL containing 25 µL/mL Geltrex®. Pictures of cysts were taken in bright field before changing medium (Invitrogen EVOS M7000, Thermofisher, France) in order to monitor growth and circularity of cysts. After 3 weeks of culture, cysts were washed twice in PBS, then fixed in 4% paraformaldehyde (PFA, Invitrogen) for 30 min at room temperature. Cysts were washed three times for 10 min in 100 mM glycine solution. Cysts were permeabilised for 5 min in a 0.5% Triton X-100 solution, then washed three times for 10 min with PBS. Unspecific site blocking was be realized by incubating for 1h in 5% BSA solution. Primary antibodies in 150 µL of 5% BSA solution were added to the wells and incubated at 4°C overnight. Wells were washed twice for 10 min in PBS, then 150 µL of fluorescent secondary antibodies were added for 1h at room temperature. Hoechst 33342 (1/1,000, Invitrogen) was used to visualize cell nuclei and Phalloidin-AF594 to visualize the F-actin network. Wells were finally washed four times with PBS, and micrographs were obtained using confocal microscopy using a 20 x objective (LEICA SP8 STED). Primary antibodies used were dedicated to identify β-catenin (Cell Signalling Technology D10A8, 1/200), E-cadherin (Invitrogen 13-1700, 1/1,000), Vimentin (Abcam ab92547, 1/100). Growth and circularity of cysts were analysed using the ImageJ software.

Western Blotting – Cells were washed with PBS and lysed in presence of a lysis buffer (50 mM Tris, pH7, 100 mM NaCl, 5 mM $MgCl_2$, 10% glycerol, 1 mM EDTA), containing 5% sodium dodecyl sulphate (SDS) and protease inhibitors (S8830, Sigma-Aldrich, France). Western blotting experiments were performed according to standard protocols. Total protein concentrations were determined using the Pierce® BCA Protein Assay Kit Thermoscientific (Fisher Scientific, France). Protein sample buffer was added and the samples were heated at 95°C for 5 min. Total protein samples were electrophoretically separated by SDS-polyacrylamide gel electrophoresis in 10% gels, and then transferred to polyvinylidene fluoride membranes (Millipore, USA). $Na_V\beta4$ proteins were detected using anti-$Na_V\beta4$ rabbit polyclonal primary antibodies (1/5,000, HPA017293, Sigma-Aldrich). Other primary antibodies used were: rabbit monoclonal anti-β-catenin (Cell Signalling Technology D10A8, 1/2,000), mouse monoclonal anti-E-cadherin (Cell Signalling Technology, 4A2, 1/2,000), rabbit monoclonal anti-Vimentin (Cell Signalling Technology, D21H3, 1/2,000), rabbit monoclonal anti-αSMA (Cell Signalling Technology, D4K9N, 1/2,000), rabbit monoclonal anti-N-Cadherin (Cell Signalling Technology, D4R1H, 1/2,000). Secondary horseradish peroxidase (HRP)-conjugated goat anti-mouse or goat anti-rabbit IgG secondary antibodies were obtained from BioRad (1/5,000) and from Jackson ImmunoResearch (1/10,000), respectively. HSC70 protein was used as a sample loading control using anti-HSC70 mouse primary antibody at 1/10,000 (Santa-Cruz). Also in some conditions, a β-actin-HRP mouse monoclonal antibody (1/1,000, SantaCruz) was used as a control for sample loading. Proteins were detected using electrochemiluminescence-plus kit (Pierce® ECL Western Blotting Substrate, Fisher Scientific, France) and captured on CL-XPosure Films (Thermoscientific, France). Densitometric analyses were performed using ImageJ software, and quantifications of proteins of interest are expressed relatively to that of the control protein used (either HSC70 or β-actin) and to the control condition. Full uncropped blots are shown in Supplementary Figure 2.

Epifluorescence experiments – MCF10A CTL and Crβ4 cells were grown for 48h in Lab-Tek™ chambers. In some cases, chambers were coated with a layer of Geltrex™ containing 25 µg/mL

of DQ-Gelatin 488. Cells were fixed in 4% paraformaldehyde for 30 min and then incubated with 5% BSA for 30 min. F-actin was visualized after staining the cells with phalloidin-AF594 (1/200, Cell Signaling Technology, France) for 1 h. Slides were mounted using ProLong® Gold Antifade Mountant with DAPI to visualize cell nuclei (Invitrogen, France). Epifluorescence microscopy was performed with an EVOS M7000 microscope (Thermofisher, France). Images were analysed using the ImageJ software.

Data presentation and statistical analysis - Data are displayed as mean ± sem when following a normal distribution, or as individual points centred by a diagram showing the median when not following a normal distribution. One-way ANOVA followed by a Dunn's Multiple Comparison Tests, two-way ANOVA, Mann-Whitney rank sum tests, paired Student t-tests were used to compare different conditions as indicated in the figure legends. Statistical significance is indicated as: *, $p < 0.05$; **, $p < 0.01$ and ***, $p < 0.001$, while "ns" stands for not statistically different.

Data availability –The authors declare that all other data supporting the findings of this study are available within the paper and its supplementary information files or available from the authors upon request.

References

AMAN, T. K., GRIECO-CALUB, T. M., CHEN, C., RUSCONI, R., SLAT, E. A., ISOM, L. L. & RAMAN, I. M. 2009. Regulation of persistent Na current by interactions between beta subunits of voltage-gated Na channels. *J Neurosci,* 29**,** 2027-42.

BANT, J. S. & RAMAN, I. M. 2010. Control of transient, resurgent, and persistent current by open-channel block by Na channel beta4 in cultured cerebellar granule neurons. *Proc Natl Acad Sci U S A,* 107**,** 12357-62.

BON, E., DRIFFORT, V., GRADEK, F., MARTINEZ-CACERES, C., ANCHELIN, M., PELEGRIN, P., CAYUELA, M. L., MARIONNEAU-LAMBOT, S., OULLIER, T., GUIBON, R., FROMONT, G., GUTIERREZ-PAJARES, J. L., DOMINGO, I., PIVER, E., MOREAU, A., BURLAUD-GAILLARD, J., FRANK, P. G., CHEVALIER, S., BESSON, P. & ROGER, S. 2016. SCN4B acts as a metastasis-suppressor gene preventing hyperactivation of cell migration in breast cancer. *Nat Commun,* 7**,** 13648.

BRACKENBURY, W. J. & ISOM, L. L. 2011. Na Channel beta Subunits: Overachievers of the Ion Channel Family. *Front Pharmacol,* 2**,** 53.

BRISSON, L., CHADET, S., LOPEZ-CHARCAS, O., JELASSI, B., TERNANT, D., CHAMOUTON, J., LERONDEL, S., LE PAPE, A., COUILLIN, I., GOMBAULT, A., TROVERO, F., CHEVALIER, S., BESSON, P., JIANG, L. H. & ROGER, S. 2020. P2X7 Receptor Promotes Mouse Mammary Cancer Cell Invasiveness and Tumour Progression, and Is a Target for Anticancer Treatment. *Cancers (Basel),* 12.

CALHOUN, J. D. & ISOM, L. L. 2014. The role of non-pore-forming beta subunits in physiology and pathophysiology of voltage-gated sodium channels. *Handb Exp Pharmacol,* 221**,** 51-89.

CHEN, C., CALHOUN, J. D., ZHANG, Y., LOPEZ-SANTIAGO, L., ZHOU, N., DAVIS, T. H., SALZER, J. L. & ISOM, L. L. 2012. Identification of the cysteine residue responsible for disulfide linkage of Na+ channel alpha and beta2 subunits. *J Biol Chem,* 287**,** 39061-9.

DAI, W., ZHOU, J., WANG, H., ZHANG, M., YANG, X. & SONG, W. 2020. miR-424-5p promotes the proliferation and metastasis of colorectal cancer by directly targeting SCN4B. *Pathol Res Pract,* 216**,** 152731.

DISS, J. K., FRASER, S. P., WALKER, M. M., PATEL, A., LATCHMAN, D. S. & DJAMGOZ, M. B. 2008. Beta-subunits of voltage-gated sodium channels in human prostate cancer: quantitative in vitro and in vivo analyses of mRNA expression. *Prostate Cancer Prostatic Dis,* 11**,** 325-33.

GILCHRIST, J., DAS, S., VAN PETEGEM, F. & BOSMANS, F. 2013. Crystallographic insights into sodium-channel modulation by the beta4 subunit. *Proc Natl Acad Sci U S A,* 110**,** E5016-24.

GONG, Y., YANG, J., WU, W., LIU, F., SU, A., LI, Z., ZHU, J. & WEI, T. 2018. Preserved SCN4B expression is an independent indicator of favorable recurrence-free survival in classical papillary thyroid cancer. *PLoS One,* 13**,** e0197007.

GRIECO, T. M., MALHOTRA, J. D., CHEN, C., ISOM, L. L. & RAMAN, I. M. 2005. Open-channel block by the cytoplasmic tail of sodium channel beta4 as a mechanism for resurgent sodium current. *Neuron,* 45**,** 233-44.

HUANG, H., QING, X. Y., ZHOU, Q., LI, H. D. & HU, Z. Y. 2021. Silencing of microRNA-3175 represses cell proliferation and invasion in prostate cancer by targeting the potential tumor-suppressor SCN4B. *Kaohsiung J Med Sci,* 37**,** 20-26.

ISOM, L. L. 2001. Sodium channel beta subunits: anything but auxiliary. *Neuroscientist,* 7**,** 42-54.

ISOM, L. L. 2002. The role of sodium channels in cell adhesion. *Front Biosci,* 7**,** 12-23.

JELASSI, B., CHANTOME, A., ALCARAZ-PEREZ, F., BAROJA-MAZO, A., CAYUELA, M. L., PELEGRIN, P., SURPRENANT, A. & ROGER, S. 2011. P2X(7) receptor activation enhances SK3 channels- and cystein cathepsin-dependent cancer cells invasiveness. *Oncogene,* 30**,** 2108-22.

JENSEN, H. H., PEDERSEN, G. A., MORGEN, J. J., PARSONS, M., PEDERSEN, S. F. & NEJSUM, L. N. 2018. The Na(+) /H(+) exchanger NHE1 localizes as clusters to cryptic lamellipodia and accelerates collective epithelial cell migration. *J Physiol*.

LENKOWSKI, P. W., SHAH, B. S., DINN, A. E., LEE, K. & PATEL, M. K. 2003. Lidocaine block of neonatal Nav1.3 is differentially modulated by co-expression of beta1 and beta3 subunits. *Eur J Pharmacol,* 467**,** 23-30.

LI, R. G., WANG, Q., XU, Y. J., ZHANG, M., QU, X. K., LIU, X., FANG, W. Y. & YANG, Y. Q. 2013. Mutations of the SCN4B-encoded sodium channel beta4 subunit in familial atrial fibrillation. *Int J Mol Med,* 32**,** 144-50.

LOPEZ-CHARCAS, O., PUKKANASUT, P., VELU, S. E., BRACKENBURY, W. J., HALES, T. G., BESSON, P., GOMORA, J. C. & ROGER, S. 2021. Pharmacological and nutritional targeting of voltage-gated sodium channels in the treatment of cancers. *iScience,* 24**,** 102270.

MCCORMICK, K. A., ISOM, L. L., RAGSDALE, D., SMITH, D., SCHEUER, T. & CATTERALL, W. A. 1998. Molecular determinants of Na+ channel function in the extracellular domain of the beta1 subunit. *J Biol Chem,* 273**,** 3954-62.

MEADOWS, L., MALHOTRA, J. D., STETZER, A., ISOM, L. L. & RAGSDALE, D. S. 2001. The intracellular segment of the sodium channel beta 1 subunit is required for its efficient association with the channel alpha subunit. *J Neurochem,* 76**,** 1871-8.

MEDEIROS-DOMINGO, A., KAKU, T., TESTER, D. J., ITURRALDE-TORRES, P., ITTY, A., YE, B., VALDIVIA, C., UEDA, K., CANIZALES-QUINTEROS, S., TUSIE-LUNA, M. T., MAKIELSKI, J. C. & ACKERMAN, M. J. 2007. SCN4B-encoded sodium channel beta4 subunit in congenital long-QT syndrome. *Circulation,* 116**,** 134-42.

MESSNER, D. J. & CATTERALL, W. A. 1985. The sodium channel from rat brain. Separation and characterization of subunits. *J Biol Chem,* 260**,** 10597-604.

MIYAZAKI, H., OYAMA, F., INOUE, R., AOSAKI, T., ABE, T., KIYONARI, H., KINO, Y., KUROSAWA, M., SHIMIZU, J., OGIWARA, I., YAMAKAWA, K., KOSHIMIZU, Y., FUJIYAMA, F., KANEKO, T., SHIMIZU, H., NAGATOMO, K., YAMADA, K., SHIMOGORI, T., HATTORI, N., MIURA, M. & NUKINA, N. 2014. Singular localization of sodium channel beta4 subunit in unmyelinated fibres and its role in the striatum. *Nat Commun,* 5**,** 5525.

MIYAZAKI, H., OYAMA, F., WONG, H. K., KANEKO, K., SAKURAI, T., TAMAOKA, A. & NUKINA, N. 2007. BACE1 modulates filopodia-like protrusions induced by sodium channel beta4 subunit. *Biochem Biophys Res Commun,* 361**,** 43-8.

O'MALLEY, H. A. & ISOM, L. L. 2015. Sodium channel beta subunits: emerging targets in channelopathies. *Annu Rev Physiol,* 77**,** 481-504.

OGINSKY, M. F., CUI, N., ZHONG, W., JOHNSON, C. M. & JIANG, C. 2017. Hyperexcitability of Mesencephalic Trigeminal Neurons and Reorganization of Ion Channel Expression in a Rett Syndrome Model. *J Cell Physiol,* 232**,** 1151-1164.

ROGER, S., GILLET, L., LE GUENNEC, J. Y. & BESSON, P. 2015. Voltage-gated sodium channels and cancer: is excitability their primary role? *Front Pharmacol,* 6**,** 152.

ROGER, S., ROLLIN, J., BARASCU, A., BESSON, P., RAYNAL, P. I., IOCHMANN, S., LEI, M., BOUGNOUX, P., GRUEL, Y. & LE GUENNEC, J. Y. 2007. Voltage-gated sodium channels potentiate the invasive capacities of human non-small-cell lung cancer cell lines. *Int J Biochem Cell Biol,* 39**,** 774-86.

SANCHEZ-SANDOVAL, A. L. & GOMORA, J. C. 2019. Contribution of voltage-gated sodium channel beta-subunits to cervical cancer cells metastatic behavior. *Cancer Cell Int,* 19**,** 35.

SHEILABI, M. A., TAKESHITA, L. Y., SIMS, E. J., FALCIANI, F. & PRINCIVALLE, A. P. 2020. The Sodium Channel B4-Subunits are Dysregulated in Temporal Lobe Epilepsy Drug-Resistant Patients. *Int J Mol Sci,* 21.

SHIMIZU, H., TOSAKI, A., OHSAWA, N., ISHIZUKA-KATSURA, Y., SHOJI, S., MIYAZAKI, H., OYAMA, F., TERADA, T., SHIROUZU, M., SEKINE, S. I., NUKINA, N. & YOKOYAMA, S. 2017. Parallel homodimer structures of the extracellular domains of the

voltage-gated sodium channel beta4 subunit explain its role in cell-cell adhesion. *J Biol Chem,* 292**,** 13428-13440.

TAN, B. H., PUNDI, K. N., VAN NORSTRAND, D. W., VALDIVIA, C. R., TESTER, D. J., MEDEIROS-DOMINGO, A., MAKIELSKI, J. C. & ACKERMAN, M. J. 2010. Sudden infant death syndrome-associated mutations in the sodium channel beta subunits. *Heart Rhythm,* 7**,** 771-8.

WHITE, H. V., BROWN, S. T., BOZZA, T. C. & RAMAN, I. M. 2019. Effects of FGF14 and NaVbeta4 deletion on transient and resurgent Na current in cerebellar Purkinje neurons. *J Gen Physiol,* 151**,** 1300-1318.

WILSON, M. J., ZHANG, M. M., AZAM, L., OLIVERA, B. M., BULAJ, G. & YOSHIKAMI, D. 2011. Navbeta subunits modulate the inhibition of Nav1.8 by the analgesic gating modifier muO-conotoxin MrVIB. *J Pharmacol Exp Ther,* 338**,** 687-93.

XIONG, H., YANG, Q., ZHANG, X., WANG, P., CHEN, F., LIU, Y., WANG, P., ZHAO, Y., LI, S., HUANG, Y., CHEN, S., WANG, X., ZHANG, H., YU, D., TAN, C., FANG, C., HUANG, Y., WU, G., WU, Y., CHENG, X., LIAO, Y., ZHANG, R., YANG, Y., KE, T., REN, X., LI, H., TU, X., XIA, Y., XU, C., CHEN, Q. & WANG, Q. K. 2019. Significant association of rare variant p.Gly8Ser in cardiac sodium channel beta4-subunit SCN4B with atrial fibrillation. *Ann Hum Genet,* 83**,** 239-248.

YANG, Q., XIONG, H., XU, C., HUANG, Y., TU, X., WU, G., FU, F., WANG, Z., WANG, L., ZHAO, Y., LI, S., HUANG, Y., WANG, C., WANG, D., YAO, Y., WANG, F., WANG, Y., XUE, Y., WANG, P., CHEN, Q., PU, J. & WANG, Q. K. 2019. Identification of rare variants in cardiac sodium channel beta4-subunit gene SCN4B associated with ventricular tachycardia. *Mol Genet Genomics,* 294**,** 1059-1071.

YU, F. H., WESTENBROEK, R. E., SILOS-SANTIAGO, I., MCCORMICK, K. A., LAWSON, D., GE, P., FERRIERA, H., LILLY, J., DISTEFANO, P. S., CATTERALL, W. A., SCHEUER, T. & CURTIS, R. 2003. Sodium channel beta4, a new disulfide-linked auxiliary subunit with similarity to beta2. *J Neurosci,* 23**,** 7577-85.

ZHANG, M. M., WILSON, M. J., AZAM, L., GAJEWIAK, J., RIVIER, J. E., BULAJ, G., OLIVERA, B. M. & YOSHIKAMI, D. 2013. Co-expression of Na(V)beta subunits alters the kinetics of inhibition of voltage-gated sodium channels by pore-blocking mu-conotoxins. *Br J Pharmacol,* 168**,** 1597-610.

Figure 1

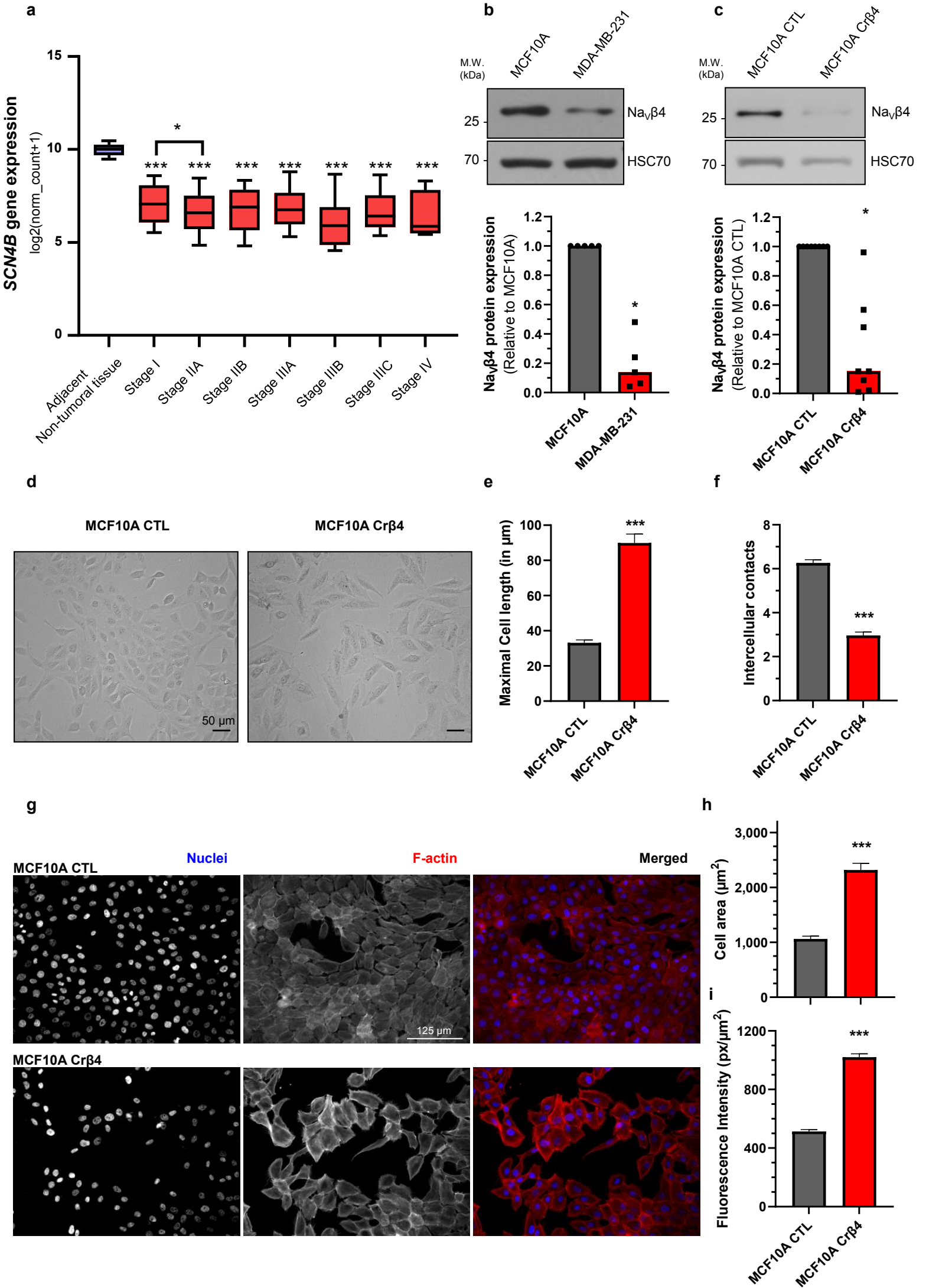
a
SCN4B gene expression
log2(norm_count+1)
15
10
5
0
*
***
Adjacent Non-tumoral tissue
Stage I
Stage IIA
Stage IIB
Stage IIIA
Stage IIIB
Stage IIIC
Stage IV
b
M.W. (kDa)
MCF10A
MDA-MB-231
25
70
NaVβ4
HSC70
NaVβ4 protein expression (Relative to MCF10A)
1.2
1.0
0.8
0.6
0.4
0.2
0.0
c
MCF10A CTL
MCF10A CrB4
NaVβ4 protein expression (Relative to MCF10A CTL)
d
MCF10A CTL
MCF10A CrB4
50 µm
e
Maximal Cell length (in µm)
100
80
60
40
20
0
f
Intercellular contacts
8
6
4
2
0
g
Nuclei
F-actin
Merged
125 µm
h
Cell area (µm²)
3,000
2,000
1,000
i
Fluorescence Intensity (px/µm²)
1200
800
400

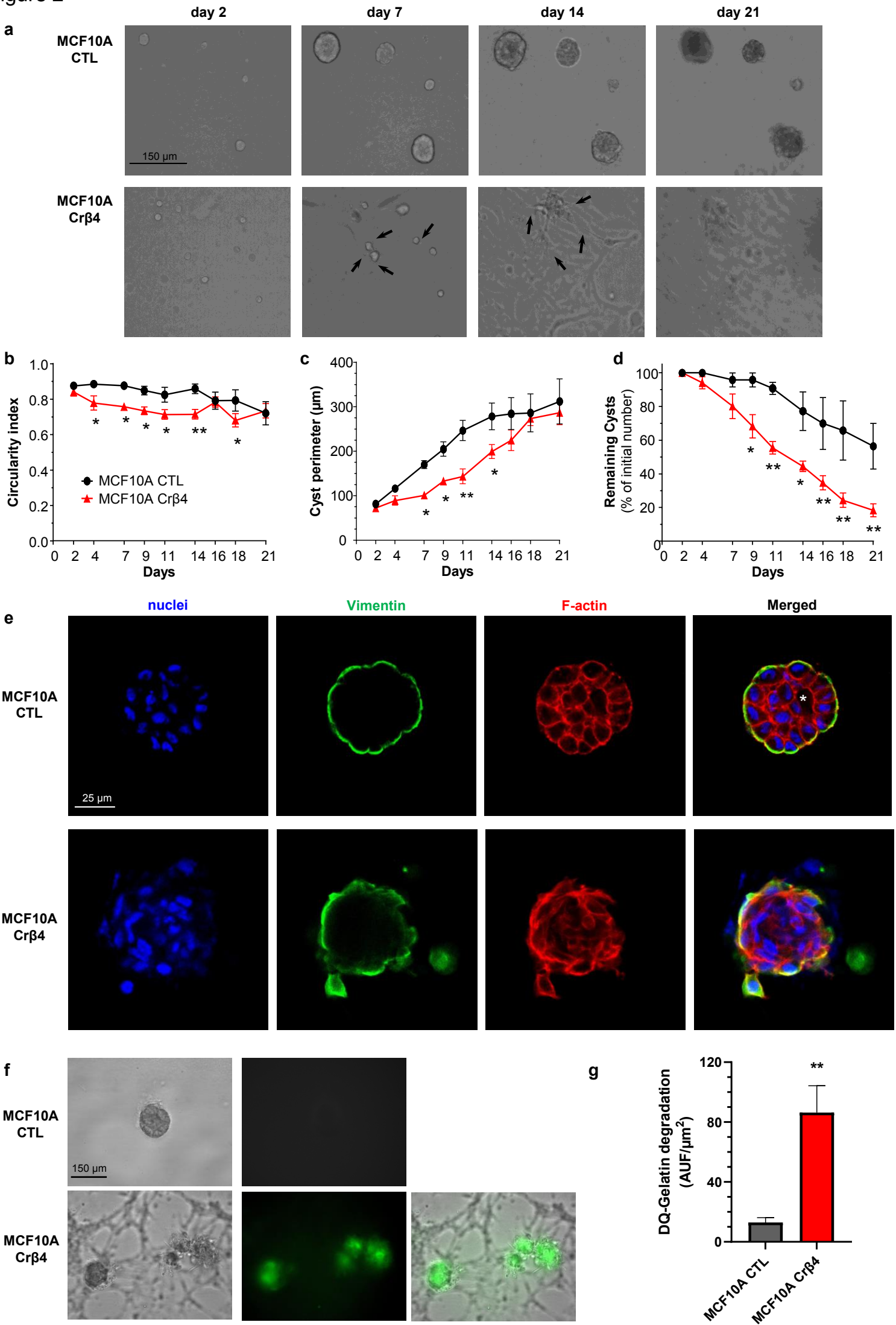
a
day 2
day 7
day 14
day 21
MCF10A CTL
MCF10A Crβ4
150 µm
b
Circularity index
MCF10A CTL
MCF10A Crβ4
Days
c
Cyst perimeter (µm)
Days
d
Remaining Cysts (% of initial number)
Days
e
nuclei
Vimentin
F-actin
Merged
MCF10A CTL
MCF10A Crβ4
25 µm
f
MCF10A CTL
MCF10A Crβ4
150 µm
g
DQ-Gelatin degradation (AUF/µm²)
MCF10A CTL
MCF10A Crβ4

Figure 3

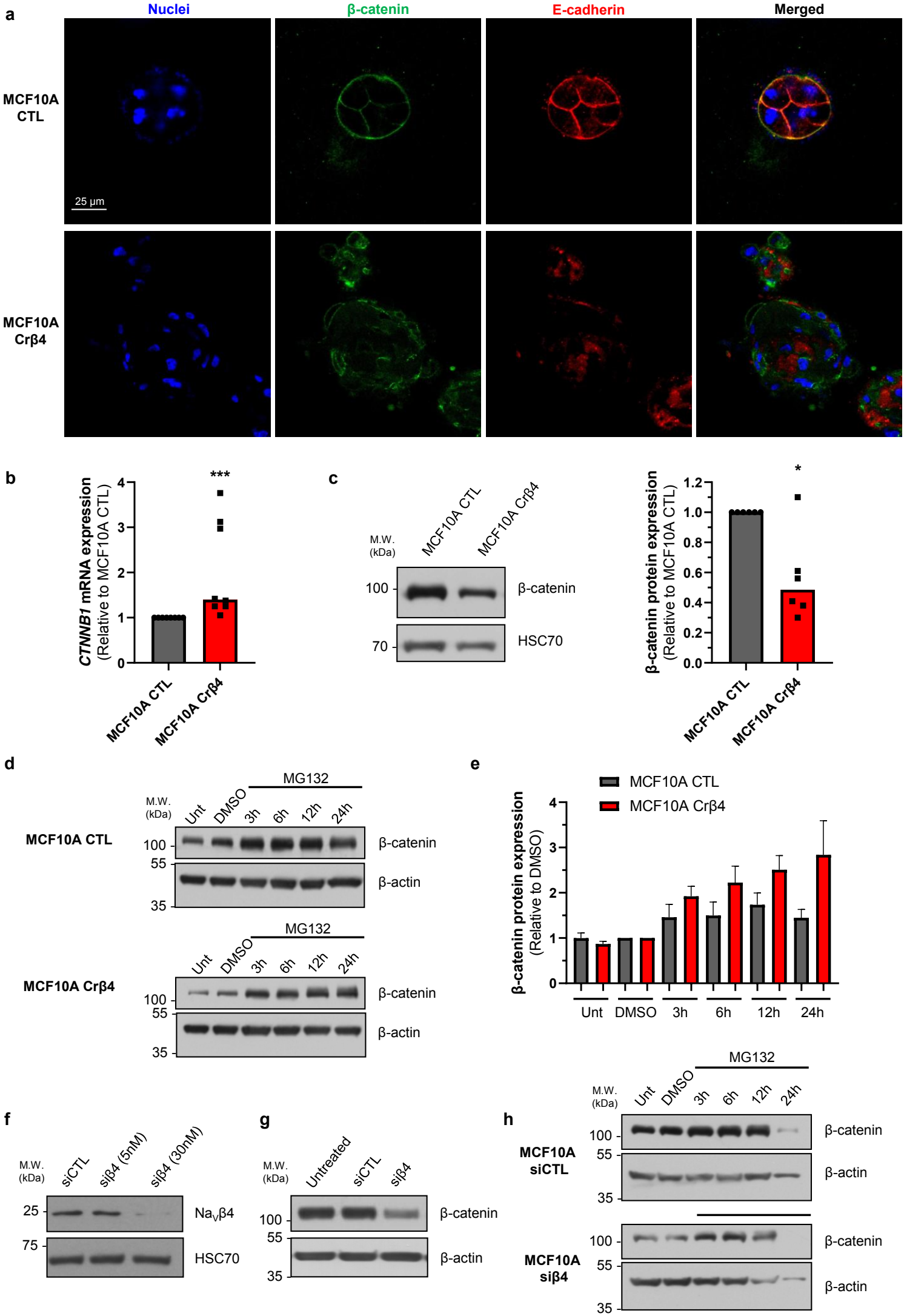
a
Nuclei
β-catenin
E-cadherin
Merged
MCF10A CTL
MCF10A Crβ4
25 µm
b
CTNNB1 mRNA expression (Relative to MCF10A CTL)
***
MCF10A CTL
MCF10A Crβ4
c
M.W. (kDa)
MCF10A CTL
MCF10A Crβ4
100
β-catenin
70
HSC70
β-catenin protein expression (Relative to MCF10A CTL)
*
d
MG132
Unt
DMSO
3h
6h
12h
24h
MCF10A CTL
MCF10A Crβ4
100
55
35
β-catenin
β-actin
e
MCF10A CTL
MCF10A Crβ4
β-catenin protein expression (Relative to DMSO)
f
siCTL
siβ4 (5nM)
siβ4 (30nM)
25
75
NaVβ4
HSC70
g
Untreated
siCTL
siβ4
100
55
35
β-catenin
β-actin
h
MG132
MCF10A siCTL
MCF10A siβ4

Figure 4

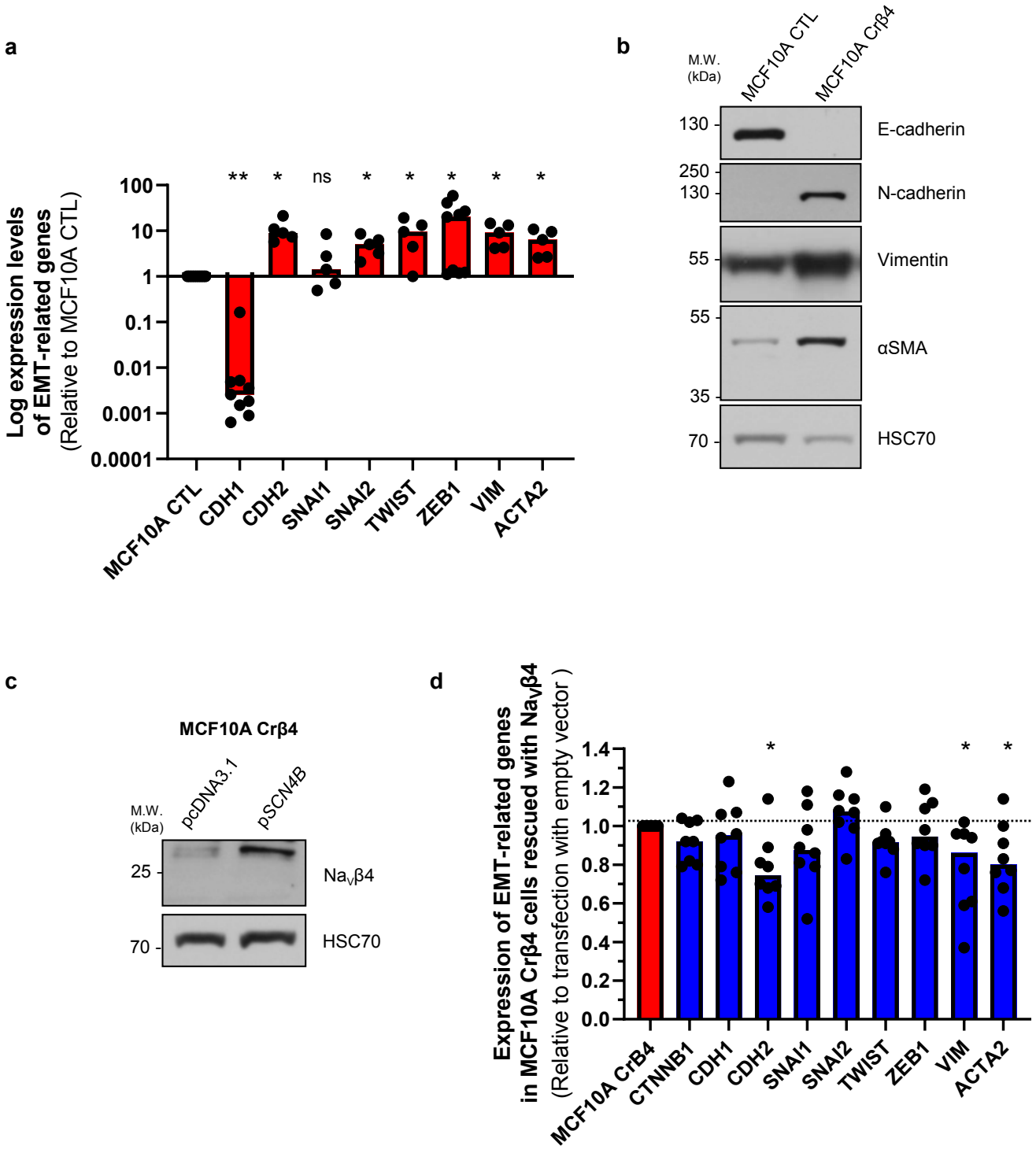
a
Log expression levels of EMT-related genes
(Relative to MCF10A CTL)
100
10
1
0.1
0.01
0.001
0.0001
** * ns * * * * *
MCF10A CTL
CDH1
CDH2
SNAI1
SNAI2
TWIST
ZEB1
VIM
ACTA2
b
M.W. (kDa)
MCF10A CTL
MCF10A Crβ4
130
E-cadherin
250
130
N-cadherin
55
Vimentin
55
35
αSMA
70
HSC70
c
MCF10A Crβ4
M.W. (kDa)
pcDNA3.1
pSCN4B
25
Nav β4
70
HSC70
d
Expression of EMT-related genes in MCF10A Crβ4 cells rescued with Nav β4
(Relative to transfection with empty vector)
1.4
1.2
1.0
0.8
0.6
0.4
0.2
0.0
* * *
MCF10A CrB4
CTNNB1
CDH1
CDH2
SNAI1
SNAI2
TWIST
ZEB1
VIM
ACTA2

Supplementary materials

THE VOLTAGE-GATED SODIUM CHANNEL BETA4 SUBUNIT MAINTAINS EPITHELIAL PHENOTYPE IN MAMMARY CELLS

Adélaïde DORAY[1], Roxane LEMOINE[1], Marc SEVERIN[2], Stéphanie CHADET[1], Osbaldo LOPEZ-CHARCAS[1], Audrey HÉRAUD[1], Christophe BARON[1], Pierre BESSON[1], Arnaud MONTEIL[3], Stine Falsig PEDERSEN[2] & Sébastien ROGER[1,4§]

[1] University of Tours, EA4245 Transplantation, Immunology, Inflammation, Tours, France

[2] Section for Cell Biology and Physiology, Department of Biology, Faculty of Science, University of Copenhagen, Copenhagen, Denmark

[3] IGF, University of Montpellier, CNRS, INSERM, Montpellier, France

[4] Institut Universitaire de France, Paris, France

[§]Correspondence: Dr. Sébastien Roger,

EA4245 Transplantation, Immunology, Inflammation, 10 Bd Tonnellé, 37032 Tours, France
Tel: (+33) 2 47 36 61 30, Email: sebastien.roger@univ-tours.fr

Supplementary Figure 1: Viability and proliferation of MCF10A CTL and MCF10A Crβ4 cells

a, MCF10A CTL and MCF10A Crβ4 cell viability was measured by the MTT assay 4 days after seeding the cells at different densities (n=6 independent experiments). *, $p<0.05$ (Wilcoxon test). **b**, Labelling with 10 μM 5-Ethynyl-2'deoxyuridine (EdU, 10 μM) in MCF10A CTL and MCF10A Crβ4 cells was assessed by flow cytometry after 3 days of culture. **c**, Analyses of results acquired as in (b) from 5 independent experiments. *, $p<0.05$ (Mann-Whitney rank sum test).

Supplementary Figure 2: uncropped WB films shown in a, Figure 1b, **b**, Figure 1c, **c,** Figure 3c, **d,** Figure 3d**, e,** Figure 3f**, f,** Figure 3g**, g,** Figure 3h**, h,** Figure 4b**,** and **f,** Figure 4c**.**

Supplementary Figure 1

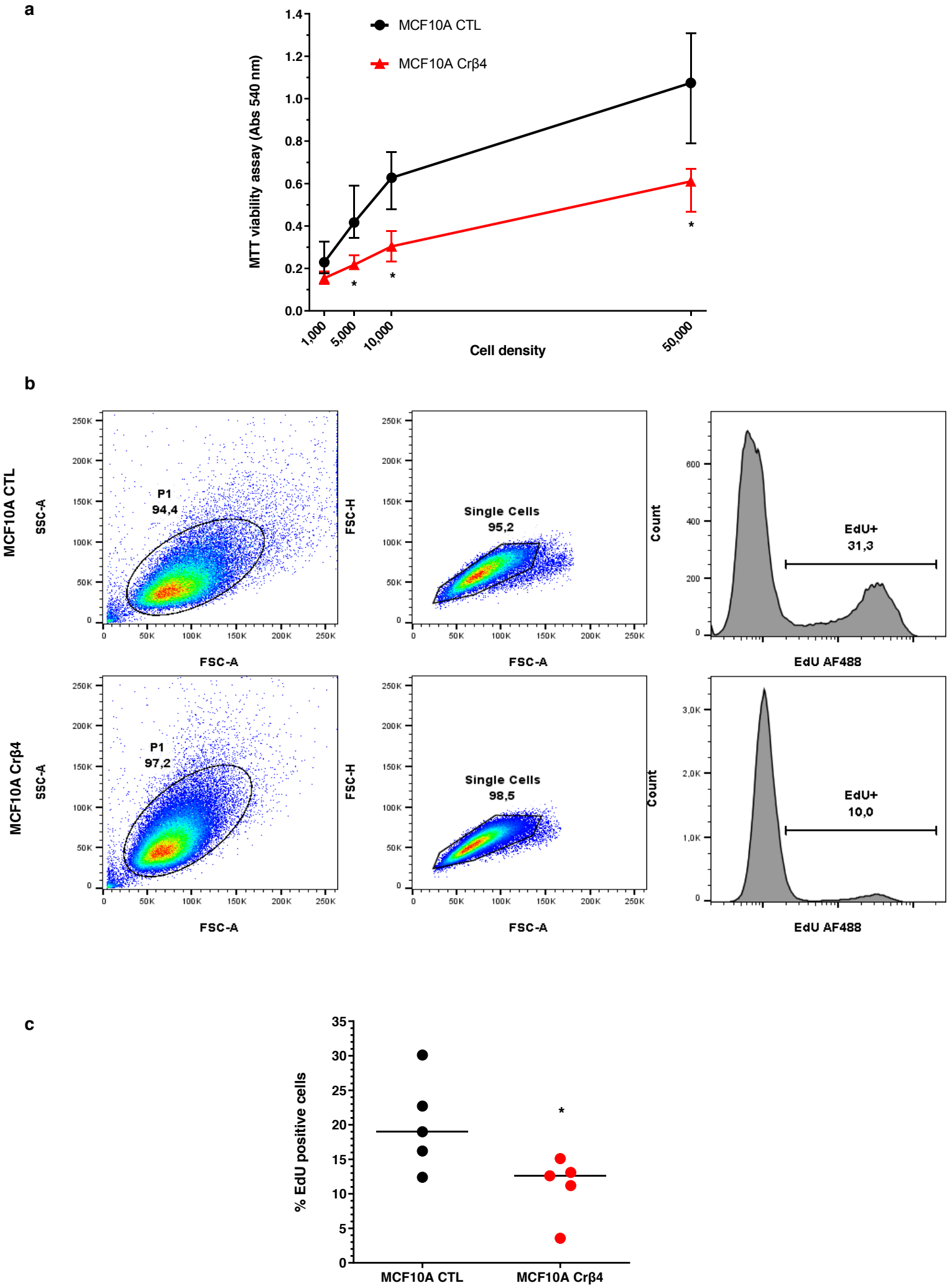

Supplementary Figure 2

a) Uncropped blots shown in figure 1a

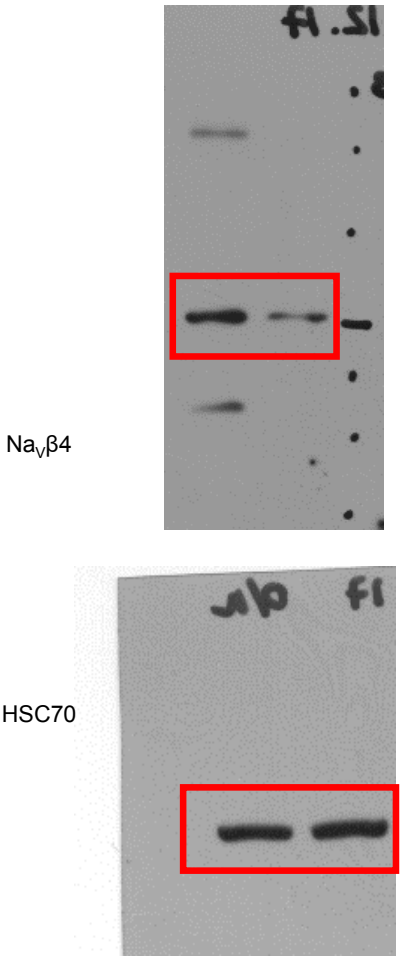

b) Uncropped blots shown in figure 1b

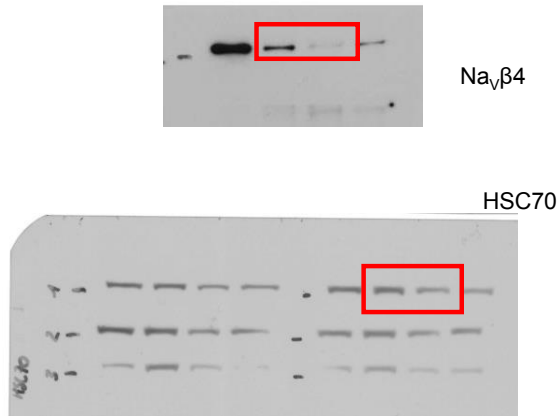

c) Uncropped blots shown in figure 3c

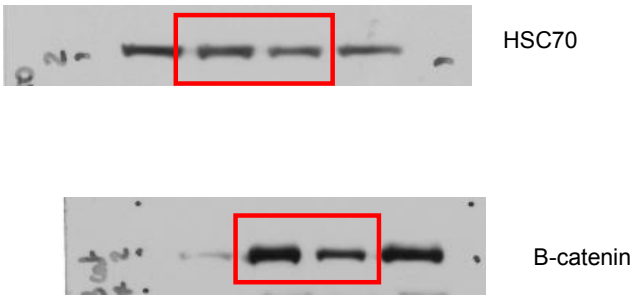

d) Uncropped blots shown in figure 3d

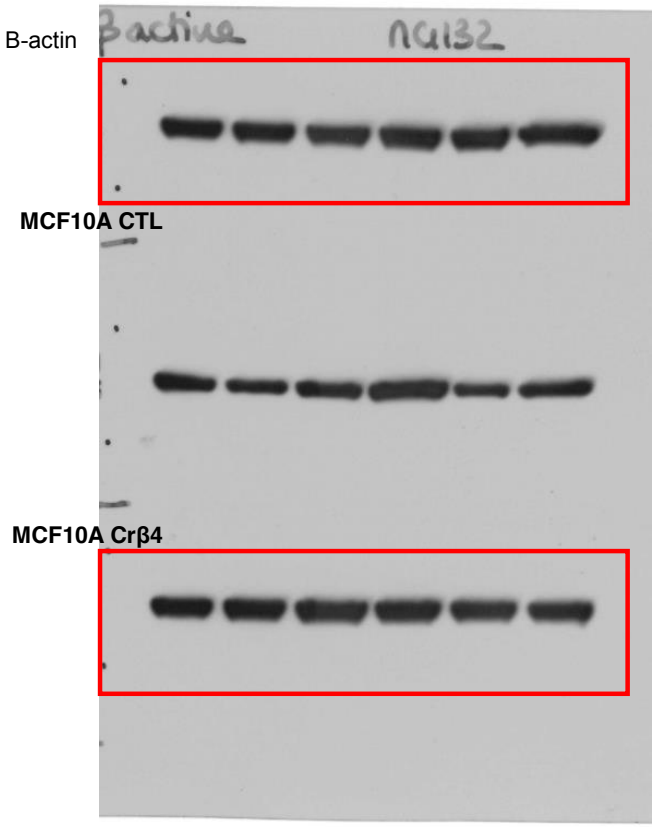

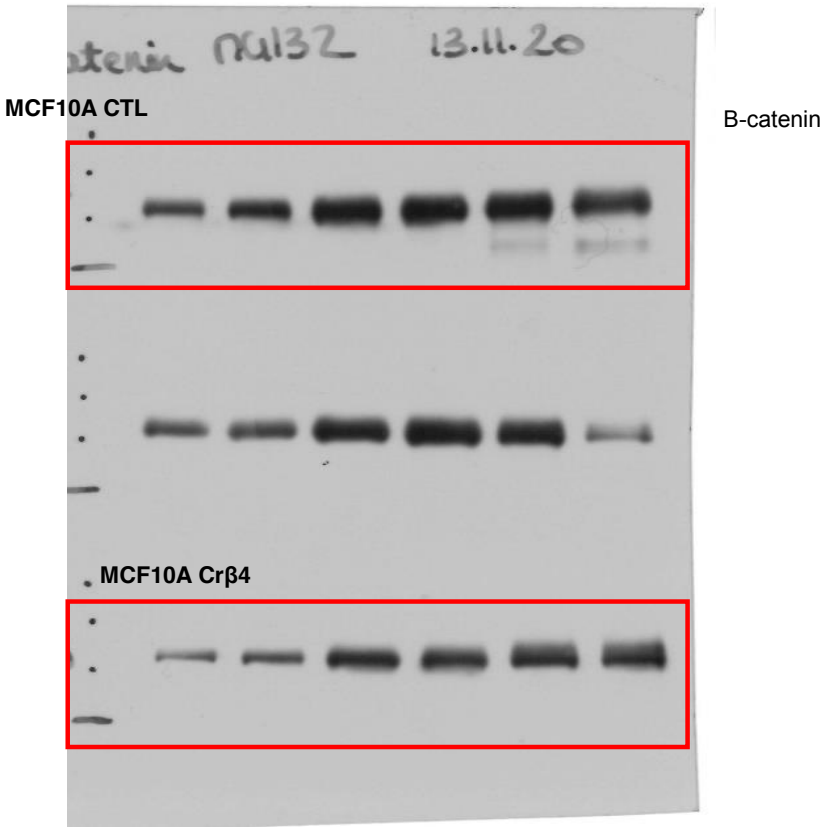

e) Uncropped blots shown in figure 3f

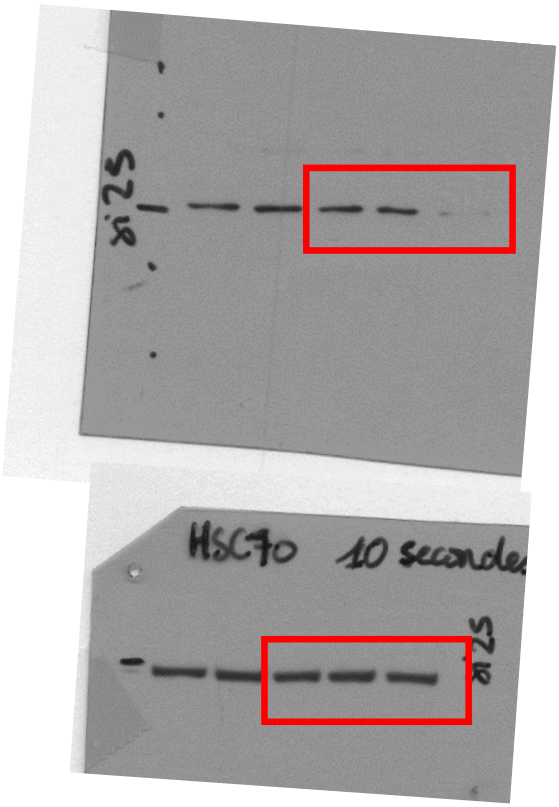

f) Uncropped blots shown in figure 3g

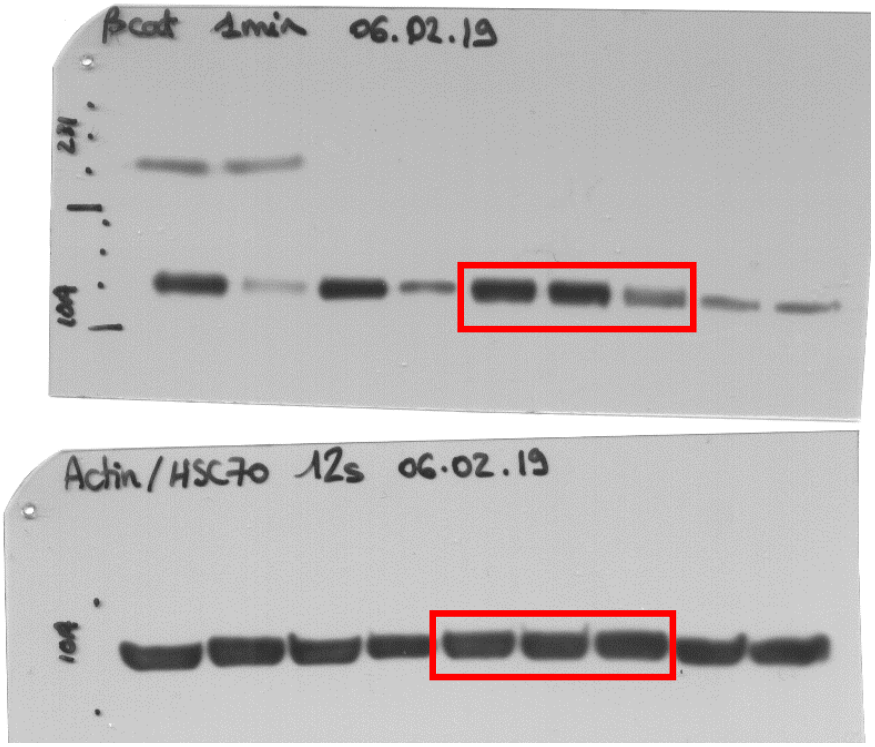

g) Uncropped blots shown in figure 3h

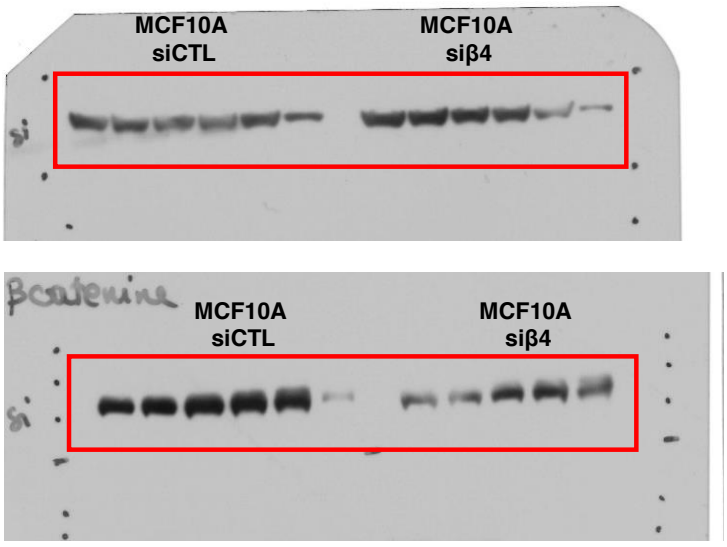

h) Uncropped blots shown in figure 4b

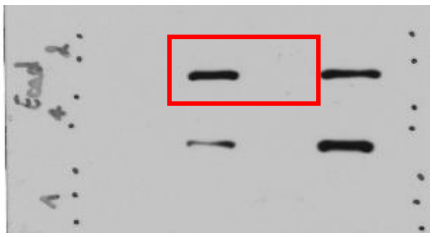

E-cadherin

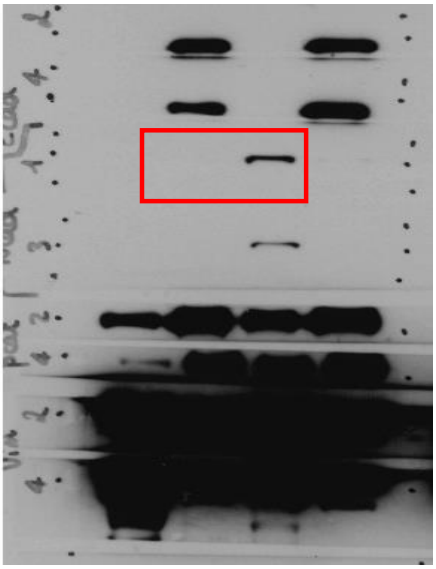

N-cadherin

Vimentin

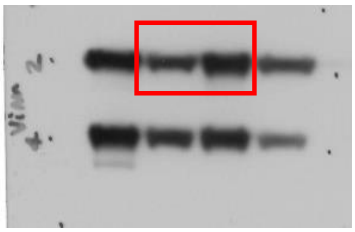

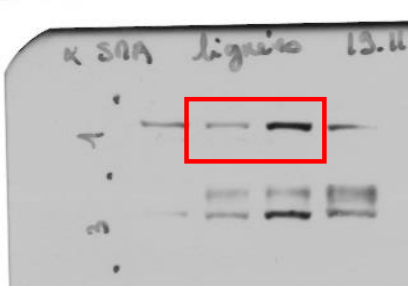

αSMA

HSC70

h) Uncropped blots shown in figure 4c

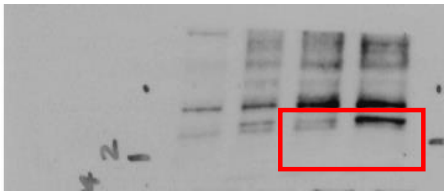

$Na_V\beta4$

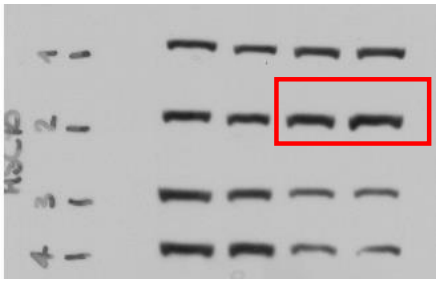

HSC70

Supplementary Table I: PCR primers used

Genes	Proteins	Forward primer (5'→3')	Reverse primer (5' →3')	Efficiencies	Expected size (pb)
CTNNB1	β-catenin	CCCACTAATGTCCAGCGTTT	GCATGATAGCGTGTCTGGAA	2.00	214
CDH1	E-cadherin	CGACCCAACCCAAGAATCTA	GGCTGTGCCTTCCTACAGAC	2.03	171
CDH2	N-cadherin	GGTGGAGGAGAAGAAGACCAG	GGCATCAGGCTCCACAGT	2.09	72
SNAI1	Snail	GGTTCTTCTGCGCTACTGCT	TAGGGCTGCTGGAAGGTAAA	2.00	157
SNAI2	Slug	GAGCATTTGCAGACAGGTCA	GCTTCGGAGTGAAGAAATGC	2.10	200
TWIST1	Twist1	CCACTGAAAGGAAAGGCATC	GCATTTTACCATGGGTCCTC	2.01	229
ZEB1	Zeb1	GCACCTGAAGAGGACCAGAG	GTGTAACTGCACAGGGAGCA	2.08	200
VIM	Vimentin	GTTTCCAAGCCTGACCTCAC	TTCCAGGGACTCATTGGTTC	1.99	246
ACTA2	α-SMA	ACCCGATAGAACATGGCATC	CATACATGGCTGGGACATTG	2.03	195
HPRT1	Hprt1	TTGCTGACCTGCTGGATTAC	TATGTCCCCTGTTGACTGGT	2.00	119